Extreme Pathway Analysis of Human Red Blood Cell Metabolism

Sharon J. Wiback and Bernhard O. Palsson
Department of Bioengineering, University of California, San Diego, La Jolla, California 92093 USA

ABSTRACT The development of high-throughput technologies and the resulting large-scale data sets have necessitated a systems approach to the analysis of metabolic networks. One way to approach the issue of complex metabolic function is through the calculation and interpretation of extreme pathways. Extreme pathways are a mathematically defined set of generating vectors that describe the conical steady-state solution space for flux distributions through an entire metabolic network. Herein, the extreme pathways of the well-characterized human red blood cell metabolic network were calculated and interpreted in a biochemical and physiological context. These extreme pathways were divided into groups based on such criteria as their cofactor and by-product production, and carbon inputs including those that 1) convert glucose to pyruvate; 2) interchange pyruvate and lactate; 3) produce 2,3-diphosphoglycerate that binds to hemoglobin; 4) convert inosine to pyruvate; 5) induce a change in the total adenosine pool; and 6) dissipate ATP. Additionally, results from a full kinetic model of red blood cell metabolism were predicted based solely on an interpretation of the extreme pathway structure. The extreme pathways for the red blood cell thus give a concise representation of red blood cell metabolism and a way to interpret its metabolic physiology.

INTRODUCTION

A constraints-based approach to the mathematical modeling and in silico study of reconstructed metabolic networks has been developed (Palsson, 2000). This approach successively imposes governing constraints on a biochemical reaction network including connectivity, thermodynamic irreversibility, and maximum flux capacities to limit the steady-state flux solutions to a closed solution space (Schilling et al., 1999, 2000). Markedly, no kinetic parameters are used in defining this space. However, if the kinetic parameters are known the precise location of the steady-state flux distribution in the solution space can be found using a model that involves simultaneously solving a system of differential equations. Such comprehensive kinetic models are available for the human red blood cell (Mulquiney and Kuchel, 1999; Lee and Palsson, 1991; Joshi and Palsson, 1989, 1990), and such a precise solution can be calculated.

Steady-state analysis of stoichiometric networks has been reviewed recently (Schilling et al., 1999) and the steady-state solution space is a convex hull, or cone, where the edges are so-called "extreme pathways." An algorithm to compute the extreme pathways has been described (Schilling et al., 2000) and applied to the genome-scale metabolic network of *Hemophilus influenzae* (Schilling and Palsson, 2000). The extreme pathways for a genome-scale network are large and challenging to both compute and interpret (Papin et al., 2002). However, the subsequent imposition of gene expression regulation significantly reduces the number of allowable extreme pathways under a given condition (Covert et al., 2001b).

Submitted January 25, 2002, and accepted for publication April 8, 2002.

Address reprint requests to Bernhard O. Palsson, 9500 Gilman Drive, La Jolla, CA 92093. Tel.: 858-534-5668; Fax: 858-822-3120; E-mail: palsson@ucsd.edu.

© 2002 by the Biophysical Society

0006-3495/02/08/808/11 $2.00

The difficulties associated with the computation and interpretation of large numbers of extreme pathways for real metabolic networks have hampered their detailed biochemical and physiological study. These computational issues arise from both the size and complexity of the metabolic networks. Although these cone-generating vectors correspond to biochemical pathways that represent steady-state flux maps, they have yet to be examined in detail for a biologically realistic metabolic system to determine their characteristics and usefulness in analyzing and interpreting integrated metabolic functions. The human red blood cell provides an attractive case to study the extreme pathways. Its metabolism contains four basic classical pathways: glycolysis, the pentose pathway, adenosine nucleotide metabolism, and the Rapoport-Leubering shunt. Unlike most metabolic networks, the red cell does not need to generate biomass; its main task is to produce the necessary cofactors (ATP, NADPH, and NADH) for maintaining its osmotic balance and electroneutrality and fighting oxidative stresses. The relatively simplistic demands on the red cell network serve to reduce the system's complexity and help make the computation of its extreme pathways manageable. The human red blood cell model accounts for 39 metabolites and 32 internal metabolic reactions, as well as 12 primary exchange and 7 currency exchange fluxes. The extreme pathways of this simple metabolic network can be readily calculated from the stoichiometric matrix. Herein we study these extreme pathways.

MATERIALS AND METHODS

The metabolic network and its stoichiometric matrix

Thirty-nine metabolites are included in the red blood cell network (Table 1). To calculate the extreme pathways, those metabolites that can be exchanged with the system boundary (both as primary exchanges and

TABLE 1 The net reactions for all type I and type II (DIS1-3) extreme pathways including both primary and currency exchange fluxes. Net reactions include system inputs (negative integers) and outputs (positive integers), and do not include internal reactions

P_#	GLC	PYR	LAC	HX	ADE	ADO	INO	23DPG	ADP	ATP	NAD	NADH	NADP	NADPH	PI	CO_2	H	NH_3	H_2O
GP1	−1	2							−2	2	−2	2			−2		2		2
GP2	−1	1							−1	1	−1	1	−6	6	−1	3	7		−2
GP3	−3	5							−5	5	−5	5	−6	6	−5	3	11		2
GP4	−2	5		1			−1		−6	6	−5	5	−4	4	−6	2	8		3
GP5	−1	2									−2	2					4		
GP6	−1	1									−1	1	−6	6		3	8		−3
GP7	−3	5									−5	5	−6	6		3	16		−3
GP8	−2	5		1			−1		−1	1	−5	5	−4	4	−1	2	13		−2
PL1		1	−1								−1	1					1		
PL2		−1	1								1	−1					−1		
DPG1	−1							2	2	−2	−2	2			−2		6		
DPG2				1			−1	1			−1	1	−4	4	−2	2	6		−2
DPG3				3			−3	5	2	−2	−5	5			−8		12		
DPG4	−1							1	1	−1	−1	1	−6	6	−1	3	9		−3
DPG5	−3							5	5	−5	−5	5	−6	6	−5	3	21		−3
DPG6	−2			1			−1	5	4	−4	−5	5	−4	4	−6	2	18		−2
IP1		5		3			−3		−8	8	−5	5			−8		2		5
IP2		1		1			−1		−2	2	−1	1	−4	4	−2	2	4		−1
IP3		5		3			−3		−3	3	−5	5			−3		7		
IP4		1		1			−1		−1	1	−1	1	−4	4	−1	2	5		−2
SP1				1	−1		1			−1					3		2	2	−5
SP2				1	−1	2	−1			−1					3		2		−3
SP3				1	−1		−1		4	−3					1				−1
GA1	−5				−6				30	−24					12		6		−6
GA2	−1				−1				5	−4			−2	2	2	1	3		−2
GA3	−5				−6		12		6	−12					24		18	12	−30
GA4	−1				−1		2		1	−2			−2	2	4	1	5	2	−6
GA5	−5				−6	12			6	−12					24		18		−18
GA6	−1				−1	2			1	−2			−2	2	4	1	5		−4
IA1						1				−1					3		2		−3
IA2							1			−1					3		2	1	−4
IA3						1			−2	1					1		1		−1
IA4							1		−2	1					1		1	1	−2
IA5						−1			3	−2									
AI1						−1	1											1	−1
AI2						−1	1		1	−1					1		1	1	−2
DIS1									1	−1					1		1		−1
DIS2									1	−1					1		1		−1
DIS3									2	−2					2		1		−2

currency exchanges) are identified (Schilling et al., 2000). Primary exchange metabolites are those that can be thought of as being transported across the cell membrane and exchanged with the environment (Fig. 1). Currency exchanges are exchanges of cofactors and metabolites that are produced and used by the metabolic network for such tasks as running the Na/K Pump (ATP), reducing met-Hemoglobin (NADH), fighting oxidative stresses to the cell via glutathione reduction (NADPH), and regulating hemoglobin oxygen affinity (2,3-DPG). The elemental composition of each metabolite in the network is given in Table 2 and it is used to ensure that every reaction in the network is elementally balanced. The metabolic reactions, excluding transporters, are shown in Table 3. The full red blood cell stoichiometric matrix is derived from these reactions and the corresponding metabolic map is shown in Fig. 1.

Extreme pathway calculation and classification

The extreme pathways are calculated based on:

$$\mathbf{S} \cdot v = \mathbf{0} \quad v_i \geq 0, \quad \forall i$$

where **S** is the red blood cell stoichiometric matrix. We constrain all fluxes (v_i) to be positive so that no reaction can be run "negatively," violating the laws of thermodynamics. Thus, reversible reactions are

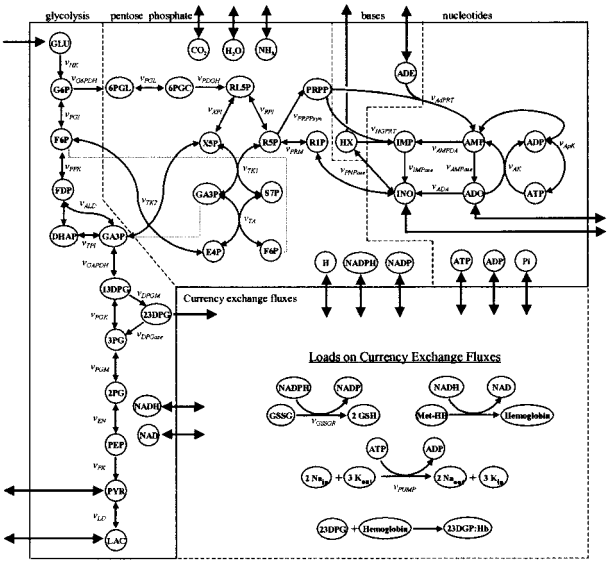

FIGURE 1 The red blood cell metabolic map depicting the classical pathways of glycolysis, the Rapoport-Leubering shunt, the pentose phosphate pathway, and adenosine metabolism (demarcated by the dashed lines). In addition, exchange fluxes with the system boundary are defined that include substrates/by-products, small molecules, and cofactors. Internal usage reactions for NADPH, NADH, ATP, and 2,3-DPG are also depicted. Note that the map does not include the F26BP bypass, which does not significantly change the extreme pathway analysis of the system; it simply adds another type II futile cycle that dissipates ATP.

broken down into their forward and backward components (Schilling and Palsson, 1998). Any steady-state flux distribution (v) within the cone can be described as a nonnegative linear combination of the extreme edges of the cone:

$$v = \sum_{i=1}^{n} \alpha_i p_i, \quad \alpha_i \geq 0$$

where the extreme pathways (p_i) are a set of generating vectors that describe a conical solution space (Schilling et al., 1999).

Extreme pathways can be divided into three main categories: type I, which are through pathways that utilize primary exchange fluxes as defined in Table 2; type II, which are futile cycles that only utilize currency exchange fluxes and degrade charged cofactors such as ATP; and type III, which are simply reversible reactions with no exchange fluxes involved (Schilling et al., 1999). Note that the type I pathways include traditional pathways with a single substrate in and a single product out, and the simultaneous production of cofactors.

RESULTS

Extreme pathway structure of the red blood cell

The computation of the extreme pathways for the red blood cell metabolic network resulted in 36 type I, 3 type II, and 16 type III extreme pathways. The type I and II extreme pathways are of most interest and will be focused on herein. The net reactions (exchanges only) are contained in Table 1 for both type I and II extreme pathways.

The type I and II extreme pathways can be described in detail based on their function and corresponding steady-state flux map. The complete collection of all 39 steady-state flux maps referred to below can be found in Fig. 5.

Glucose to pyruvate (GP)

These pathways show three basic routes from glucose to pyruvate: classic glycolysis (GP1), glycolysis and cyclic pentose phosphate metabolism (PPP) (GP2), and glycolysis and PPP (GP3). GP1 produces the standard two ATP, two NADH, and two pyruvate from one glucose molecule. GP3 enters the PPP (bypassing PGI) where carbon is lost to CO_2 but NADPH is produced. The net result is a decrease in the net production of ATP, NADH, and pyruvate per glucose molecule, as compared to GP1, in exchange for the production of the glutathione reducing cofactor NADPH. GP2 takes GP3 a step further and actually cycles through PPP repeatedly, causing an even greater loss of carbon through the decarboxylation reaction of PDGH, but an increase in the production of NADPH in addition to the single ATP, NADH, and pyruvate formed per glucose molecule. Each of these three pathways has a nearly identical twin pathway (GP5, GP6, GP7) that utilizes the 2,3-DPG shunt (DPGM and DPGase) as opposed to the ATP producing reaction catalyzed by PGK. The cell can use the shunt to curb its ATP production. GP4 supplements the glucose substrate with inosine to ultimately produce the cofactors ATP, NADH, and NADPH, as well as pyruvate. However, due to the low transport rate of inosine (V_{max} in Table 3), this is a low-flux pathway. GP4 has a mirror image pathway (GP8) in which the 2,3-DPG shunt is utilized instead of PGK.

Pyruvate/lactate conversion (PL)

Pathways PL1 and PL2 represent the reversible conversion between pyruvate and lactate that can occur in the cell and ultimately is used to balance the NAD/NADH ratio. Note that in the homeostatic steady state there is no load on NADH and the red blood cell utilizes PL2 to completely balance all NADH produced via any GP pathways utilized.

2,3-DPG production (DPG)

The basic routes of four of these pathways (DPG1 and DPG4–6) are identical to those from group I (GP5–8), the only difference being that instead of simply diverting flux through the shunt and back into main glycolysis, 2,3-DPG is siphoned off for use in the regulation of the oxygen affinity of hemoglobin. In addition, DPG2 and DPG3 utilize inosine

TABLE 2 A list of all 39 metabolites included in the red blood cell model

Int.	P. Ex.	C. Ex.	Abbreviation	Metabolite	Empirical Formula
	×		GLC	Glucose	C6 H12 O6
×			G6P	Glucose-6-phosphate	C6 H11 O9 P1
×			F6P	Fructose-6-phosphate	C6 H11 O9 P1
×			FDP	Fructose-1,6-phosphate	C6 H10 O12 P2
×			DHAP	Dihydroxyacetone phosphate	C3 H5 O6 P1
×			GA3P	Glyceraldehyde-3-phosphate	C3 H5 O6 P1
×			13DPG	1,3-Diphosphoglycerate	C3 H4 O10 P2
		×	23DPG	2,3-Diphosphoglycerate	C3 H3 P2 O10
×			3PG	3-Phosphoglycerate	C3 H4 O7 P1
×			2PG	2-Phosphoglycerate	C3 H4 O7 P1
×			PEP	Phosphoenolpyruvate	C3 H2 O6 P1
	×		PYR	Pyruvate	C3 H3 O3
	×		LAC	Lactate	C3 H5 O3
×			6PGL	6-Phosphogluco-lactone	C6 H9 O9 P1
×			6PGC	6-Phosphogluconate	C6 H10 O10 P1
×			RL5P	Ribulose-5-phosphate	C5 H9 O8 P1
×			X5P	Xylulose-5-phosphate	C5 H9 O8 P1
×			R5P	Ribose-5-phosphate	C5 H9 O8 P1
×			S7P	Sedoheptulose-7-phosphate	C7 H13 O10 P1
×			E4P	Erythrose-4-phosphate	C4 H7 O7 P1
×			PRPP	5-Phosphoribosyl-1-pyrophosphate	C5 H8 O14 P3
×			IMP	Inosine monophosphate	C10 N4 H12 O8 P1
×			R1P	Ribose-1-phosphate	C5 H9 O8 P1
	×		HX	Hypoxanthine	C5 N4 H4 O1
	×		INO	Inosine	C10 H12 N4 O5
	×		ADE	Adenine	C5 H5 N5
	×		ADO	Adenosine	C10 H13 N5 O4
×			AMP	Adenosine monophosphate	C10 N5 H13 O7 P1
		×	ADP	Adenosine diphosphate	C10 N5 H13 O10 P2
		×	ATP	Adenosine triphosphate	C10 N5 H13 O13 P3
		×	NAD	Nicotinamide adenine dinucleotide	NAD
		×	NADH	Nicotinamide adenine dinucleotide (R)	NAD H1
		×	NADP	Nicotinamide adenine dinucleotide phosphate	NADP
		×	NADPH	Nicotinamide adenine dinucleotide phosphate (R)	NADP H1
	×		H	Hydrogen Ion	H1
	×		Pi	Inorganic Phosphate	H1O4 P1
	×		NH3	Ammonia	N1 H3
	×		CO2	Carbon Dioxide	C1 O2
	×		H2O	Water	H2 O1

Each metabolite is categorized as internal (Int.), primary exchange (P. Ex.), or currency exchange (C. Ex.). The empirical formula is included for each metabolite (Lehninger et al., 1993; Stryer, 1988).

as the sole substrate, with no uptake of glucose (similar to IP3 and IP4 described below).

Inosine to pyruvate (IP)

These pathways (IP1–4) mirror GP1, GP2, GP5, and GP6, respectively, with the only difference being that inosine is used as the sole substrate instead of glucose. Inosine is converted, via adenosine metabolism, into R5P, which enters pentose phosphate metabolism and is eventually converted into pyruvate via glycolysis. Again, these are low-flux pathways due to the low transport rate for inosine.

Salvage pathways using adenine (SP)

The salvage pathways (SP1–3) combine adenine with a pentose to alter the adenosine nucleotide pool inventory.

Nucleotide incorporation/removal via glucose and adenine (GA)

These pathways (GA1–6) use glucose and adenine to adjust the nucleotide pool size via either the oxidative or non-oxidative branch of the PPP.

Nucleotide incorporation/removal via inosine and adenosine (IA)

Similar to the SP group, these pathways (IA1–4) regulate the adenosine pool size through the uptake/secretion of inosine and adenosine.

Adenosine to inosine (AI)

These two pathways (AI1–2) simply convert adenosine to inosine for use in nucleotide metabolism.

TABLE 3 The 32 internal metabolic reactions included in the model

Abbreviation	Enzyme	Chemical Reaction	Elemental Representation of Chemical Equation	V_{max}, mM/h
Glycolysis and Rapoport-Leubering Shunt				
HK	Hexokinase	GLU + ATP → G6P + ADP + H	C6 H12 O6 + C10 H13 P3 O13 N5 = C6 H11 P1 O9 + C10 H13 P2 O10 N5 + H	12
PGI	Phosphoglucoisomerase	G6P ↔ F6P	C6 H11 P1 O9 = C6 H11 P1 O9	
PFK	Phosphofructokinase	F6P + ATP → FDP + ADP + H	C6 H11 P1 O9 + C10 H13 P3 O13 N5 = C6 H10 P2 O12 + C10 H13 P2 O10 N5 + H	250
ALD	Aldolase	FDP ↔ GA3P + DHAP	C6 H10 P2 O12 = C3 H5 P1 O6 + C3 H5 P1 O6	
TPI	Triose phosphate isomerase	DHAP ↔ GA3P	C3 H5 P1 O6 = C3 H5 P1 O6	
GAPDH	Glyceraldehyde phosphate dehydrogenase	GA3P + NAD + Pi ↔ 13DPG + NADH + H	C3 H5 P1 O6 + NAD + HPO4 = C3 H4 P2 O10 + NAD-H + H	
PGK	Phosphoglycerate kinase	13DPG + ADP ↔ 3PG + ATP	C3 H4 P2 O10 + C10 H13 P2 O10 N5 = C3 H4 P1 O7 + C10 H13 P3 O13 N5	
DPGM	Diphosphoglyceromutase	13DPG → 23DPG + H	C3 H4 P2 O10 = C3 H3 P2 O10 + H	12
DPGase	Diphosphoglycerate phosphatase	23DPG + H2O → 3PG + Pi	C3 H3 P2 O10 + H2O = C3 H4 P1 O7 + HPO4	0.52
PGM	Phosphoglyceromutase	3PG ↔ 2PG	C3 H4 P1 O7 = C3 H4 P1 O7	
EN	Enolase	2PG ↔ PEP + H2O	C3 H4 P1 O7 = C3 H2 P1 O6 + H2O	
PK	Pyruvate kinase	PEP + ADP + H → PYR + ATP	C3 H2 P1 O6 + C10 H13 P2 O10 N5 + H = C3 H3 O3 + C10 H13 P3 O13 N5	250
LD	Lactate dehydrogenase	PYR + NADH + H ↔ LAC + NAD	C3 H3 O3 + NAD-H + H = C3 H5 O3 + NAD	
Pentose Phosphate Pathway				
G6PDH	Glucose-6-phosphate dehydrogenase	G6P + NADP → 6PGL + NADPH + H	C6 H11 P1 O9 + NADP = C6 H9 P1 O9 + NADP-H + H	189
PGL	6-phosphoglyconolactonase	6PGL + H2O ↔ 6PGC + H	C6 H9 P1 O9 + H2O = C6 H10 P1 O10 + H	1440
PDGH	6-phosphoglyclononate dehydrogenase	6PGC + NADP → RL5P + NADPH + CO2	C6 H10 P1 O10 + NADP = C5 H9 P1 O8 + NADP-H + CO2	265
RPI	Ribose-5-phosphate isomerase	RL5P ↔ R5P	C5 H9 P1 O8 = C5 H9 P1 O8	
XPI	Xylulose-5-phosphate epimerase	RL5P ↔ X5P	C5 H9 P1 O8 = C5 H9 P1 O8	
TKI	Transketolase	X5P + R5P ↔ S7P + GA3P	C5 H9 P1 O8 + C5 H9 P1 O8 = C7 H13 P1 O10 + C3 H5 P1 O6	
TA	Transaldolase	GA3P + S7P ↔ E4P + F6P	C3 H5 P1 O6 + C7 H13 P1 O10 = C4 H7 P1 O7 + C6 H11 P1 O9	
TKII	Transketolase	X5P + E4P ↔ F6P + GA3P	C5 H9 P1 O8 + C4 H7 P1 O7 = C6 H11 P1 O9 + C3 H5 P1 O6	
Adenosine Nucleotide Metabolism				
PRPPsyn	Phosphoribosyl pyrophosphate synthetase	R5P + ATP → PRPP + AMP	C5 H9 P1 O8 + C10 H13 P3 O13 N5 = C5 H8 P3 O14 + C10 H13 P1 O7 N5 + H	0.55
PRM	Phosphoribomutase	R1P ↔ R5P	C5 H9 P1 O8 = C5 H9 P1 O8	
HGPRT	Hypoxanthine guanine phosphoryl transferase	PRPP + HX + H2O → IMP + 2Pi	C5 H8 P3 O14 + C5 H4 O1 N4 + H2O = C10 H12 P1 O8 N4 + 2*HPO4	0.2
AdPRT	Adenine phosphoribosyl transferase	PRPP + ADE + H2O → AMP + 2Pi	C5 H8 P3 O14 + C5 H5 N5 + H2O = C10 H13 P1 O7 N5 + 2*HPO4	0.08
PNPase	Purine nucleoside phosphorylase	INO + Pi ↔ HX + R1P	C10 H12 O5 N4 + HPO4 = C5 H4 O1 N4 + C5 H9 P1 O8	
IMPase	Inosine monophosphatase	IMP + H2O → INO + Pi + H	C10 H12 P1 O8 N4 + H2O = C10 H12 O5 N4 + HPO4 + H	
AMPDA	Adenosine monophosphate deaminase	AMP + H2O → IMP + NH3	C10 H13 P1 O7 N5 + H2O = C10 H12 P1 O8 N4 + NH3	0.01
AMPase	Adenosine monophosphate phosphohydrolase	AMP + H2O → ADO + Pi + H	C10 H13 P1 O7 N5 + H2O = C10 H13 O4 N5 + HPO4 + H	
ADA	Adenosine deaminase	ADO + H2O → INO + NH3	C10 H13 O4 N5 + H2O = C10 H12 O5 N4 + NH3	20
AK	Adenosine kinase	ADO + ATP → ADP + AMP	C10 H13 O4 N5 + C10 H13 P3 O13 N5 = C10 H13 P2 O10 N5 + C10 H13 P1 O7 N5	2.4
ApK	Adenylate kinase	2 ADP ↔ ATP + AMP	C10 H13 P2 O10 N5 + C10 H13 P2 O10 N5 = C10 H13 P3 O13 N5 + C10 H13 P1 O7 N5	

As shown via the elemental representation, all small molecules including water and hydrogen are accounted for in the reaction definitions. V_{max} is included for enzymes where it is known. Note that V_{max} values for many of the transport reactions were calculated based on the nominal internal and external concentrations for each exchange metabolite. Values taken from Joshi and Palsson (1990).
Transporters end their V_{max} values (in mM/h): inosine, 0.1; pyruvate, 1.08; lactate, 3.3; adenine, 0.01; adenosine, 0.03; hypoxanthine, 13.

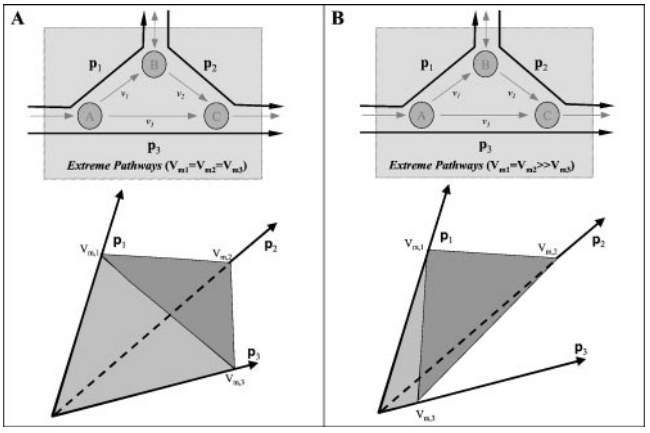

FIGURE 2 The three extreme pathways of this sample system form a conical solution space. (*A*) Full capabilities of the system where the cone is capped off at the minimum V_{max} for each pathway; (*B*) A simulation of an enzymopathy in which the maximum flux capacity of v_3 is greatly reduced. This reduction in the maximum capacity results in a shift down the p_3 axis, thus significantly shrinking the size and volume of the steady-state solution cone, and hence the metabolic capabilities of the system.

Dissipation of ATP (type II pathways, DIS)

These futile cycles (DIS1–3) serve to dissipate excess ATP

Maximal fluxes through the extreme pathways

Maximum flux capacities of the reactions serve to "cap off" the steady-state solution cone forming a closed polytope (Fig. 2 *A*). Every reaction has an estimated absolute V_{max} value of 1×10^6 molecules/s/μm^3 set by physico-chemical limitations. However, a few enzymes in the metabolic network will have a lower maximum flux capacity, i.e., low V_{max} due to kinetic limitations of the enzyme (Table 3). The enzyme with the lowest V_{max} in an extreme pathway serves as the "bottleneck" and determines the maximum possible flux through that extreme pathway. For instance, the low uptake rate of inosine limits the fluxes through all the extreme pathways in which it is utilized.

Response to metabolic loads in red blood cell metabolism

There are four main physiologic loads experienced by the red blood cell, and the extreme pathways can be interpreted in terms of these metabolic demands.

1. ATP loads are a combination of the Na/K ATPase-driven pump used in osmotic and ion balance as well as general ATP-related cell maintenance. ATP loads are experienced at the normal physiologic steady state as the pump must constantly be run and cellular volume maintained. Such loads are modeled by the conversion of ATP to ADP and P_i. Hence, some combination of extreme pathways that convert ADP to ATP must be utilized, which includes the GPs and the IPs, which is consistent with the nominal steady state in which ~80% of the flux in the system is through glycolysis (GP1 and GP5), ~15% is through the PPP (GP2–4, GP6–8), and the rest is through the adenosine reactions (IP1–4). If ATP is produced by the system in excess, it can be dissipated via one of the type II futile cycle pathways (DIS1–3);
2. Oxidative loads in the red blood cell are combated via glutathione reduction, which must then be reoxidized by NADPH. There is a basal level of oxidative load on the cell at the physiologic steady state. Oxidative loads are modeled via the oxidation of NADPH to NADP. Because NAPDH can only be produced in the oxidative branch of the PPP, pathways GP2–4 and/or GP6–8 must be utilized;
3. 2,3-DPG loads are experienced in conditions such as high altitude, where the oxygen affinity of hemoglobin must be altered. However, at the physiologic steady state there is no drain on 2,3-DPG. The only pathways that produce 2,3-DPG which can be drained from the system are DPG1–6 which, while not "turned on" in nominal steady state, will become active under load;
4. NADH loads are used to convert the unusable form of methylated hemoglobin (met-Hb) into the oxygen-carrying form of hemoglobin. Under normal, steady-state conditions, however, there is no drain on NADH. Hence, all the extreme pathways that result in the production of pyruvate are not technically utilized (GP1–8 and IP1–4). Rather, these pathways function in tandem with PL2 to balance NADH and produce lactate (Fig. 3). Note that such combinations of extreme pathways lie on a "face" of the conical solution space and represent an elementary flux mode (Schuster et al., 2000).

Extreme pathways and the interpretation of physiological responses

The stoichiometry of a metabolic network, and hence the extreme pathway structure of that network, is relatively easy to obtain as compared with acquiring detailed kinetic knowledge about each enzyme in the network. A number of valuable physiological insights can be obtained from network structure and basic reaction capacity limitations, as the following examples demonstrate.

Projection of pathways based on production of key cofactors

The high-dimensional steady-state flux cone as defined by the extreme pathways can be projected onto a 2-D flux space (see Fig. 4 *A*, *inset*). A projection of interest, Fig. 4 *A*, shows ATP and NADPH production by extreme pathways, which can be interpreted by the fluxes through the ATP and NADPH use reactions (Fig. 1).

The normal usages of ATP and NADPH in the red blood cell are ~1.5 and 0.3 mM/h, respectively. These usage rates

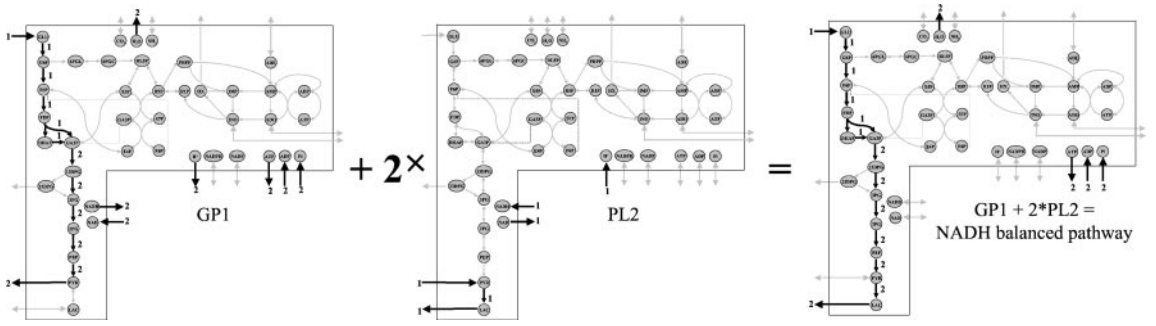

FIGURE 3 Extreme pathways GP1 and PL2 can be "added" to produce a pathway on the face of the solution cone (an elementary mode) that balances NADH, as is the case in the physiologic steady state of the red blood cell.

are indicated in Fig. 4 *A* as the physiological steady state. The projected extreme pathways that are closest to the estimated physical steady state are GP1, GP2, and GP3. A nonnegative linear combination of these pathways engulfs the physiological steady state with a "load margin," as indicated. Thus, the red blood cell would be able to meet challenges of approximately an additional 0.4 and 3.0 mM/h loads on ATP and NADPH individually, or a combination thereof, as indicated in the figure. Since a detailed kinetic model of RBC metabolism is available (Jamshidi et al., 2001) one can also dynamically determine the load margin. The discrete points in Fig. 4 *A* indicate the load margin of red blood cell metabolism based on a full kinetic model. Thus, the extreme pathway structure and enzyme capacities alone can conservatively determine the ability of the red blood cell to withstand metabolic challenges.

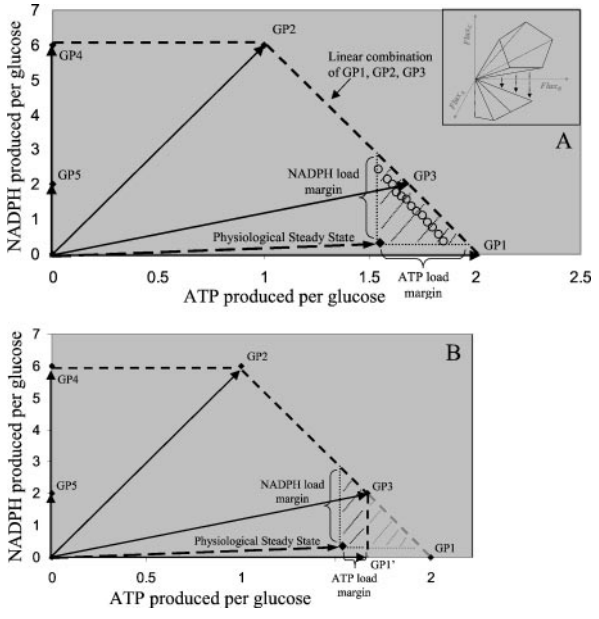

FIGURE 4 *Inset:* A schematic of how a high-dimensional cone can be projected into a 2-D plane. (*A*) Projection of the red blood cell high-dimensional flux cone as defined by the extreme pathways into a 2-D cofactor space. The nominal steady-state value is shown by the dashed arrow. The red blood cell's capacity to respond to loads (*hatched region*) is defined as the difference between the steady-state operating point (*black diamond*) and the edge of the solution space representing the maximum capabilities of the cell (*dotted line*). Any loads outside the solution space are not attainable. The results from repeated dynamic simulation of stepwise increasing energy and oxidative loads on the red blood cell are plotted on the graph with open black circles using the Jamshidi model (Jamshidi et al., 2001). Note that the kinetic model is slightly more restrictive than the stoichiometric one. (*B*) 2-D projection into the cofactor space in which an enzymopathy has shortened GP1 to GP1′ (decreased the minimum V_{max}). The cell's ability to respond to energy loads (*black hatched region*) is decreased as compared with the normal cell (*gray hatched region*).

Change in global adenosine inventory in the red blood cell

There are several extreme pathways that lead to a net change in the adenosine inventory (i.e., [A] + [AMP] + [ADP] + [ATP]), including SP1–3, GA1–6, and IA1–5. The flux through these extreme pathways is restricted to between 0.01 and 0.03 mM/h because they are all limited by one or more low effective V_{max} reactions, including adenine (ADE) and adenosine (ADO) transport, and the internal deaminase reaction catalyzed by AMPDA (Table 3). The steady-state adenosine inventory in the red blood cell is ~3 mM, and thus the time constant associated with changes in the inventory is (3 mM)/(0.01 mM/h) ~ 300 h ~ 12 days. The slow changes in the adenosine inventory in red blood cells is known and represents a challenge in blood storage (Grimes, 1980).

Adjustment in 2,3-DPG concentration

All the pathways that drain the pool of 2,3-DPG must go through DPGase whose flux is restricted to ~0.5 mM/h (Werner and Heinrich, 1985). Given that the approximate concentration of 2,3-DPG in red blood cells is 5 mM, this leads to an estimated 10 h time constant for changes in 2,3-DPG concentration and concomitant adjustment in hemoglobin oxygen affinity.

SNPs and maximal capacities

The V_{max} values of the enzymes serve to "cap off" the steady-state solution cone (Fig. 2). Changes or alterations in

these V_{max} values can significantly change the shape of the steady-state solution space. If all the extreme pathways are high throughput (i.e., limiting V_{max} is large), the solution space is relatively large (Fig. 2 *A*). However, as shown in Fig. 2 *B*, if one of the V_{max} values is low due to some sort of defect or significant kinetic regulation, the volume of the solution space shrinks significantly, which reduces the number of steady-state solutions and hence the number of homeostatic options available to the cell. Thus, V_{max} values can effectively reduce the solution space and eliminate a large number of possible states of the network. Any enzymopathies that reduce this capacity region will result in a pathological phenotype in response to challenges that normal red blood cells would tolerate (Fig. 4 *B*). Well-defined polymorphisms reduce the ability of the red blood cell to respond to oxidative and energy loads (Nagel, 1988; Beutler, 1986). Regulation of gene expression in prokaryotes can be interpreted in this way as well (Covert et al., 2001b).

DISCUSSION

Extreme pathway analysis has been applied to the human red blood cell metabolic network. The resulting extreme pathways were analyzed and classified based on their structure and functional capabilities. The results of this study are 1) the establishment of a complete set of extreme pathways for a biologically meaningful system, 2) the finding that some of the extreme pathways correspond to "classical" biochemical pathways but most do not, and 3) a demonstration that extreme pathways can be used to interpret the steady-state solution space with respect to network capabilities.

Previously, extreme pathway analysis was applied to sample systems without real biological meaning (Schilling et al., 2000). Such systems helped in establishing the algorithm and interpreting the results, but provided no real biological insight. At the other extreme, the analysis has been applied to genome-scale metabolic network, resulting in an immense number of extreme pathways for which a detailed interpretation is not possible. Only statistical properties of these large sets of data could be obtained yielding limited insight into cellular physiology (Papin et al., 2002). This red blood cell study represents a situation where the full set of extreme pathways was calculated, detailed, and used for physiological interpretation. Scaling such detailed analysis to a genome-scale represents an unmet challenge in this field.

The systemic extreme pathways of the red blood cell metabolic network were fully enumerated and described (Fig. 5). In contrast to traditional experimental discovery and heuristic definitions of metabolic pathways, extreme pathway analysis provides a unique, mathematically defined way to identify systemically meaningful metabolic pathways that may be unintuitive, but no less informative. Interestingly, "historical" pathways such as glycolysis (GP1 in Fig. 5) and nucleotide salvage pathways (SP1–3 in Fig. 5) are extreme pathways. However, a majority of the extreme pathways are nontraditional multiple input-multiple output pathways such as those in which glucose and inosine are used in tandem to produce pyruvate and hypoxanthine, as well as the cofactors ATP and NADH (GP4 in Fig. 5). Such nontraditional pathways are an example of how extreme pathway analysis can elucidate systemic properties resulting from network interconnectedness and complexity, an essential feature of emerging systems biology.

Extreme pathway analysis can also be used to interpret and predict the systemic consequences of maximum capabilities of individual reactions in the network (Fig. 4 *A*); a priori, a seemingly impossible task for a model based solely on stoichiometric information. In this case, the maximum cofactor production capacity of the red blood cell was conservatively predicted by the extreme pathway structure and the tolerance to elevated metabolic demands defined. The incorporation of basic transport and reaction V_{max} values and approximate metabolite concentration data expands the utility of extreme pathway analysis to include estimation of time constants with respect to pathway usage and prediction of the effect of enzyme defects on systemic function (Fig. 4 *B*).

With the emergence of systems biology comes a need for new methods for defining and understanding metabolic pathways as they pertain to network-scale functions. A recent article by Marcotte begs the question: "Why not abandon the old representation of pathways and instead work directly with the networks?" (Marcotte, 2001). Many different methods for such pathway definitions have been proposed to understand whole-cell metabolism, including Ouzounis's database definitions (Ouzounis and Karp, 2000), Schuster's elementary flux modes (Schuster et al., 1999, 2000), and Schilling's extreme pathways (Schilling et al., 2000). Such computational methods are essential for providing the link between mathematics and biology. Extreme pathways provide a unique way to define metabolic pathways in the era of systems biology. The main challenges that currently face extreme pathway analysis are their computation for genome-scale networks and the physiological interpretation of the results.

The present study represents the first complete analysis of the extreme pathway structure of a real metabolic system. Previously, the extreme pathway algorithm has either been applied to simple example systems for which the pathways could be interpreted but were not physiologically relevant, or to a genome-scale model for which the pathways were most certainly meaningful but were simply too numerous to individually interpret. The human red blood cell provides an ideal test bed that combines simplicity with physiologic significance. The results from the extreme pathway analysis show that network structure and capacity constraints provide a strong basis for analysis and interpretation of the physiology of the red blood cell metabolic network. Ge-

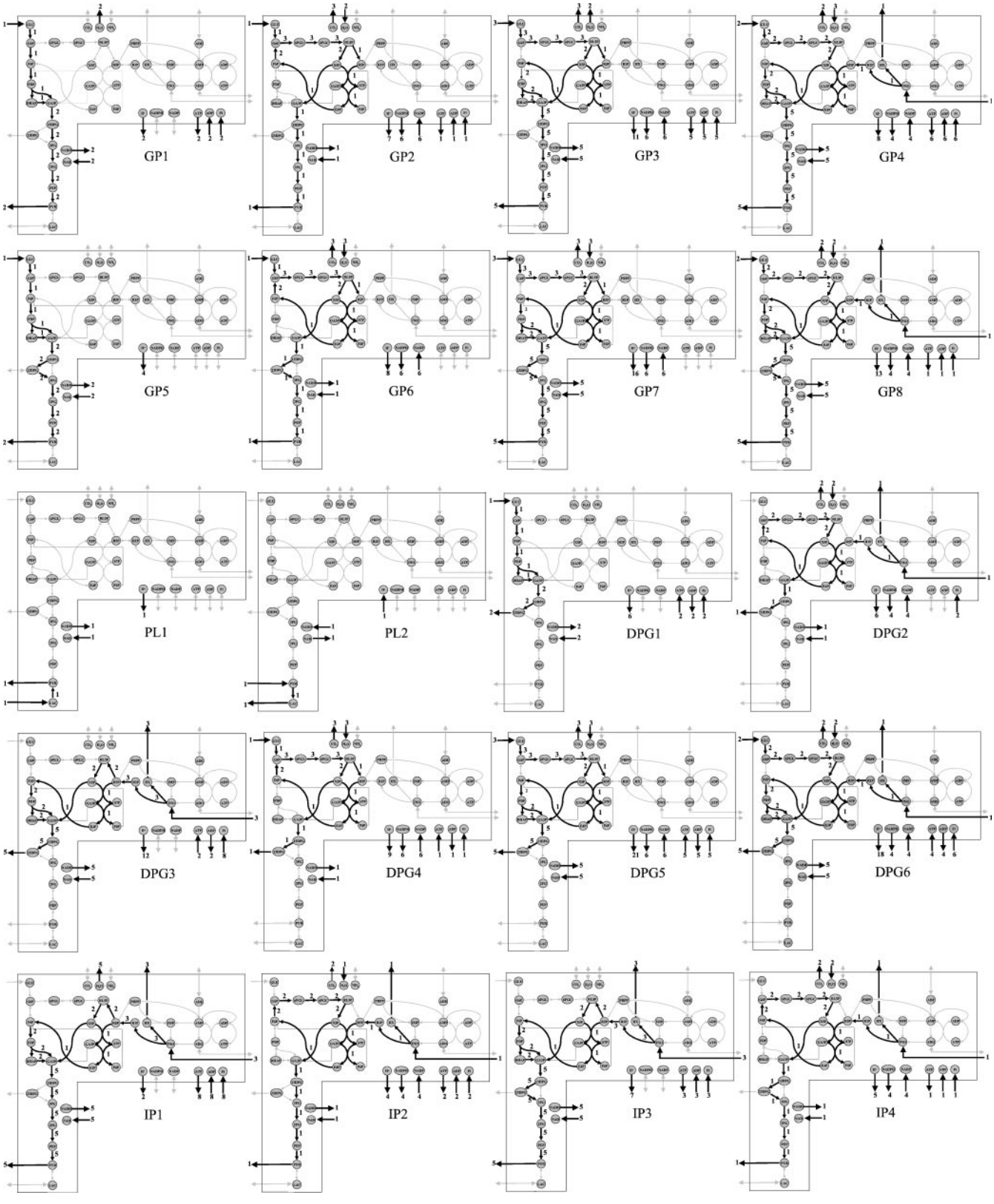

FIGURE 5 Steady-state flux maps for all type I and type II red blood cell extreme pathways.

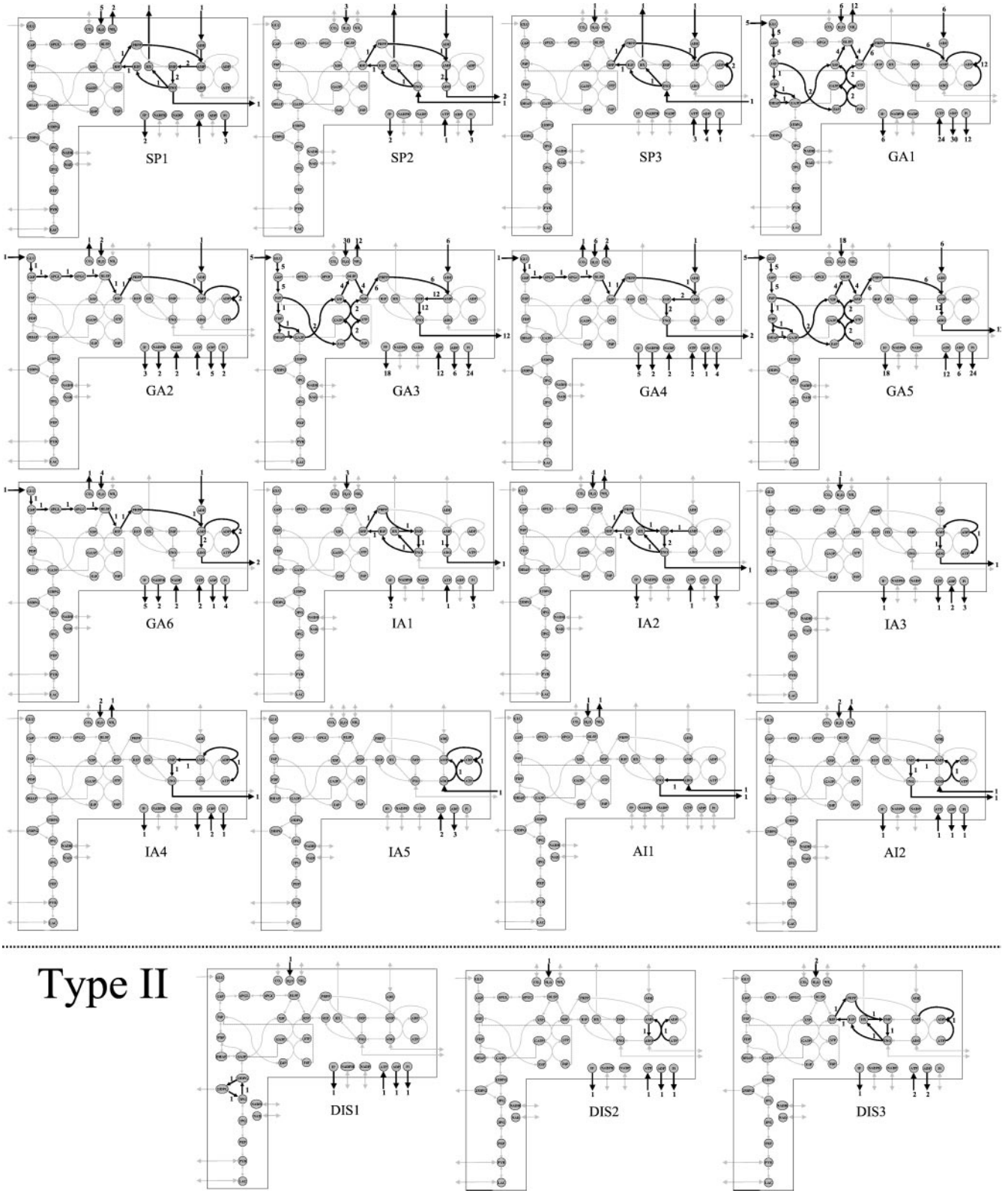

FIGURE 5 (Continued)

nome-scale metabolic networks can now be reconstructed from genomic and other data sources (Covert et al., 2001a). The use of extreme pathways for the analysis of such reconstructed networks and their relation to whole-cell functions will thus become critical in the advancement of systems biology.

The authors thank Iman Famili and Neema Jamshidi for valuable discussions and help with the figures.

This work is funded by the National Science Foundation (Graduate Research Fellowships BES98-14092, MCB98-73384, and BES-0120363) and the National Institutes of Health (Grant GM57089).

REFERENCES

Beutler, E. 1986. Red Cell Metabolism. Churchill Livingstone; Edinburgh, New York.

Covert, M. W., C. H. Schilling, I. Famili, J. S. Edwards, I. I. Goryanin, E. Selkov, and B. O. Palsson. 2001a. Metabolic modeling of microbial strains in silico. *Trends Biochem. Sci.* 26:179–186.

Covert, M. W., C. H. Schilling, and B. Palsson. 2001b. Regulation of gene expression in flux balance models of metabolism. *J. Theor. Biol.* 213: 73–88.

Grimes, A. J. 1980. Human Red Cell Metabolism. Blackwell Scientific Publications, Oxford.

Jamshidi, N., J. S. Edwards, T. Fahland, G. M. Church, and B. O. Palsson. 2001. Dynamic simulation of the human red blood cell metabolic network. *Bioinformatics.* 17:286–287.

Joshi, A., and B. O. Palsson. 1989. Metabolic dynamics in the human red cell. I. A comprehensive kinetic model. *J. Theor. Biol.* 141:515–528.

Joshi, A., and B. O. Palsson. 1990. Metabolic dynamics in the human red cell. II. Metabolic reaction rates. *J. Theor. Biol.* 142:41–68.

Lee, I.-D., and B. O. Palsson. 1991. A comprehensive model of human erythrocyte metabolism: extensions to include pH effects. *Biomed. Biochim. Acta.* 49:771–789.

Lehninger, A. L., M. M. Cox, and D. L. Nelson. 1993. Principles of Biochemistry. Worth Publishers, New York.

Marcotte, E. M. 2001. The path not taken. *Nat. Biotechnol.* 19:626–627.

Mulquiney, P. J., and P. W. Kuchel. 1999. Model of 2,3-bisphosphoglycerate metabolism in the human erythrocyte based on detailed enzyme kinetic equations: computer simulation and metabolic control analysis. *Biochem. J.* 34(2 Pt 3):597–604.

Nagel, R. L. 1988. Genetically Abnormal Red Cells. CRC Press, Boca Raton, Fla.

Ouzounis, C. A., and P. D. Karp. 2000. Global properties of the metabolic map of *Escherichia coli*. *Genome Research.* 10:568–576.

Palsson, B. O. 2000. The challenges of in silico biology. *Nat. Biotechnol.* 18:1147–1150.

Papin, J. A., N. D. Price, J. S. Edwards, and B. O. Palsson. 2002. The genome-scale metabolic extreme pathway structure in *Haemophilus influenzae* shows significant network redundancy. *J. Theor. Biol.* 215: 67–82.

Schilling, C. H., D. Letscher, and B. O. Palsson. 2000. Theory for the systemic definition of metabolic pathways and their use in interpreting metabolic function from a pathway-oriented perspective. *J. Theor. Biol.* 203:229–248.

Schilling, C. H., and B. O. Palsson. 1998. The underlying pathway structure of biochemical reaction networks. *Proc. Natl. Acad. Sci. U.S.A.* 95:4193–4198.

Schilling, C. H., and B. O. Palsson. 2000. Assessment of the metabolic capabilities of *Haemophilus influenzae* Rd through a genome-scale pathway analysis. *J. Theor. Biol.* 203:249–283.

Schilling, C. H., S. Schuster, B. O. Palsson, and R. Heinrich. 1999. Metabolic pathway analysis: basic concepts and scientific applications in the post-genomic era. *Biotechnol. Prog.* 15:296–303.

Schuster, S., T. Dandekar, and D. A. Fell. 1999. Detection of elementary flux modes in biochemical networks: a promising tool for pathway analysis and metabolic engineering. *Trends Biotechnol.* 17:53–60.

Schuster, S., D. A. Fell, and T. Dandekar. 2000. A general definition of metabolic pathways useful for systematic organization and analysis of complex metabolic networks. *Nat. Biotechnol.* 18:326–332.

Stryer, L. 1988. Biochemistry. W. H. Freeman, New York.

Werner, A., and R. Heinrich. 1985:A kinetic model for the interaction of energy metabolism and osmotic states of human erythrocytes. Analysis of the stationary “in vivo” state and of time dependent variations under blood preservation conditions. *Biomed. Biochim. Acta.* 44:185–212.